Published in final edited form as:

Nature. 2017 October 05; 550(7674): 128–132. doi:10.1038/nature24028.

Discovery of a potent catalytic p300/CBP inhibitor that targets lineage-specific tumors

Loren M. Lasko[1,*], **Clarissa G. Jakob**[1,*], **Rohinton P. Edalji**[1], **Wei Qiu**[1], **Debra Montgomery**[1], **Enrico L. Digiammarino**[1], **T. Matt Hansen**[1], **Roberto M. Risi**[1], **Robin Frey**[1], **Vlasios Manaves**[1], **Bailin Shaw**[1], **Mikkel Algire**[1], **Paul Hessler**[1], **Lloyd T. Lam**[1], **Tamar Uziel**[1], **Emily Faivre**[1], **Debra Ferguson**[1], **Fritz G. Buchanan**[1], **Ruth L. Martin**[1], **Maricel Torrent**[1], **Gary G. Chiang**[1,2], **Kannan Karukurichi**[3], **J. William Langston**[4], **Brian T. Weinert**[5], **Chunaram Choudhary**[5], **Peter de Vries**[6], **John H. Van Drie**[7], **David McElligott**[8], **Ed Kesicki**[3], **Ronen Marmorstein**[9], **Chaohong Sun**[1], **Philip A. Cole**[10], **Saul H. Rosenberg**[1], **Michael R. Michaelides**[1], **Albert Lai**[1,11], and **Kenneth D. Bromberg**[1,11]

[1]Discovery, Global Pharmaceutical Research and Development, AbbVie, 1 North Waukegan Road, North Chicago, Illinois 60064

[2]eFFECTOR Therapeutics, 11180 Roselle St., Suite A, San Diego, CA 92121

[3]Petra Pharma Corporation, 430 E. 29th St., Suite 435, New York, NY 10016

[4]Faraday Pharmaceuticals, 1616 Eastlake Ave E, Suite 560 Seattle, WA 98102

[5]Department of Proteomics, the Novo Nordisk Foundation Center for Protein Research, Faculty of Health and Medical Sciences, University of Copenhagen, Blegdamsvej 3B, DK-2200 Copenhagen, Denmark

[6]Cascadian Therapeutics, Inc., 2601 Fourth Avenue, Suite 500, Seattle, WA 98121

[7]Van Drie Research, 109 Millpond, Andover, MA 01845

[8]Accelerator Corporation, 430 East 29th St., New York, NY 10106

[11]Corresponding Authors: Kenneth D. Bromberg (kenneth.bromberg@abbvie.com); Albert Lai (Albert.Lai@abbvie.com).
*These authors contributed equally to this study

Data Availability

Structural data that support the findings of this study have been deposited in PDB with the accession code **5KJ2**, and microarray data have been deposited in GEO with the accession code **GSE94580**. All other data that support the findings of this study are provided as graph source data for Figures 1–4 and Extended data Figures 1,5–8, and 10, as Supplementary Data (Supplementary Tables 1–16, Supplementary Figure 1) or can be made available by the authors upon a reasonable request.

Author Contributions

J.V.D. developed and conducted the virtual ligand screen (VLS) and K.K. performed the screening of the VLS hits and analysis. T.M.H., R.R., R.F., and M.R.M. designed compounds. M.T. generated 3D protein homology models and small molecule docking/computational models. R.P.E produced protein, W.Q. produced protein crystals, and C.G.J. performed X-ray structure determination and analysis. E.D. performed surface plasmon resonance experiments and analysis. K.K., V.M. and M.A. performed *in vitro* biochemical studies. K.D.B. and L.M.L. performed cellular acetyl and methyl mark high content microscopy assays. B.S., D.M., J.W.L, L.M.L., L.L., and K.D.B. performed cellular sensitivity, qPCR, and western blotting experiments and analysis. B.T.W. and C.C. performed auto-acetylation mass spectrometry experiments. P.H., L.L., and T.U. performed microarray experiments and analysis. E.F. performed ChIP experiments and analysis. D.F. and F.G.B. performed *in vivo* xenograft experiments. D.M., J.W.L., P.D.V., E.K., R.M., P.C., G.G.C, C.S., M.R.M, S.R., A.L., and K.D.B designed studies and interpreted results. K.D.B. and M.R.M wrote the paper.

Supplementary Information is linked to the online version of the paper at www.nature.com/nature.

[9]Perelman School of Medicine, University of Pennsylvania, 421 Curie Blvd., Philadelphia, PA 19104

[10]Johns Hopkins University, 725 N. Wolfe St., Baltimore, MD 21205

Summary

The dynamic and reversible acetylation of proteins catalyzed by histone acetyltransferases (HATs) and histone deacetylases (HDACs) is a major epigenetic regulatory mechanism of gene transcription [1] associated with multiple diseases. While HDAC inhibitors are approved to treat certain cancers, progress on the development of drug-like HAT inhibitors has lagged [2]. The HAT paralogs p300 and CBP (p300/CBP) are key transcriptional co-activators essential for a multitude of cellular processes and also implicated in human pathological conditions, including cancer [3]. Current p300/CBP HAT domain inhibitors including natural products, [4] bi-substrate analogs (Lys-CoA) [5] and the widely utilized C646 [6, 7] lack potency or selectivity. Here, we describe A-485, a potent, selective and drug-like p300/CBP catalytic inhibitor. We show the first high resolution (1.95Å) co-crystal structure of a small molecule bound to the catalytic active site of p300 and demonstrate that A-485 is acetyl-CoA competitive. A-485 selectively inhibited proliferation across lineage-specific tumor types, including several hematological malignancies and androgen receptor-positive prostate cancer. A-485 inhibited the androgen receptor transcriptional program in both androgen sensitive and castrate resistant prostate cancer and inhibited tumor growth in a castration resistant xenograft model. These results demonstrate the feasibility of selectively targeting the catalytic activity of histone acetyltransferases.

Keywords

EP300; CBP; H3K27Ac; histone acetyltransferase; prostate cancer; androgen receptor

To identify novel small molecule inhibitors of p300, we conducted a virtual ligand screen based on compound docking to the Lys-CoA binding pocket in a proposed open conformation (Supplementary Table 1). Approximately 800,000 compounds were screened *in silico* and ca. 1,300 commercially available compounds were tested in a direct radioactive p300/CBP HAT assay. This led to two confirmed hits, the hydantoin 1 (1) and the conjugated thiazolidinedione 2 (2), which were similar to previously described hits Rtt109 [8] and C375, [6] respectively (Fig. 1a). Optimization of 1 focused on improving enzymatic and cellular activity, generating the amine-substituted indane spirooxazolidinedione Compound R (3) (Fig. 1a). Conversion to a urea improved microsomal stability and deactivating potential sites of metabolism via fluorine substitution gave rise to A-485 (4) and the inactive analog A-486 (5). A-485 was at least 1000-fold more potent than other previously described p300 cell permeable tool compounds including C646 [6] (Supplementary Table 2), which was inactive at concentrations up to 10 μM under our assay conditions.

To further characterize the ability of A-485 to inhibit p300 HAT activity, we utilized a time-resolved fluorescence resonance energy transfer (TR-FRET) assay measuring acetylation of a biotinylated histone H4 peptide. A-485 inhibited the activity of the p300-BHC (bromodomain-HAT-C/H3) domain (IC_{50} = 9.8 nM) as well as CBP-BHC (IC_{50} = 2.6 nM)

(Fig. 1b,c, similar results were observed in the absence of EDTA, Extended Data Fig.1a). In contrast, the inactive analog A-486 was ~1000-fold less potent toward p300 (IC_{50} > 10,000 nM) and CBP (IC_{50} = 9,032 nM). Surface plasmon resonance experiments indicated that A-485 bound to p300-HAT with a K_D = 15±1 nM (S.D.) and displayed a slow off-rate (k_{off} = 1.3±0.01e-03/s, $t_{1/2}$ = 531±4.5 s), (Fig. 1d), while A-486 bound to p300-HAT ~1,000-fold more weakly (K_D = 20,000±1000 nM) and a very fast off-rate (k_{off} > 0.3/s) (Fig. 1e). To provide additional evidence that A-485 binds to p300-BHC, we determined via a thermal shift assay that both Lys-CoA and A-485 increased the thermostability of p300-BHC by 5.8 °C (Extended Data Fig. 1b). A-485 was assayed against other HAT family members and did not inhibit the activity of PCAF, HAT1, MYST3, MYST4, TIP60 and GCN5L2 at 10 μM (Supplementary Table 3) and was selective over BET bromodomain proteins (Supplementary Table 4) and >150 non-epigenetic targets (Supplementary Tables 5–7). The compound only displayed substantial binding (>90%) to dopamine and serotonin transporters at 10 μM along with modest inhibition of Plk3 (IC_{50}=2.7 μM). As A-485 does not achieve significant brain exposure (Supplementary Table 13), it is unlikely to modulate these transporters *in vivo*.

To definitively establish the binding mode and delineate specific interactions of A-485 with p300, we determined the X-ray crystal structure of the fully active human p300 HAT domain (1287 to 1666 with auto-inhibitory internal loop deletion of amino acids 1523–1554 plus K1637R and M1652G mutations (Δp300 HAT), in complex with A-485 at 1.95Å resolution (data collection shown in Extended Data Fig. 2). Comparison with structures of the inactive Δp300 HAT Y1467F mutant in complex with acetyl-CoA [9] (Extended Data Fig. 1c) or the bi-substrate inhibitor Lys-CoA [10] (Fig. 2a) confirms that the A-485 binding site overlaps with that for acetyl-CoA, but not the peptide substrate binding site. Additionally, two molecules of Δp300 HAT are oriented such that Lys-1558 of one molecule inserts into the lysine substrate tunnel of a symmetry related molecule (Extended Data Fig. 3), highlighting the inherent accessibility of the inhibitor-bound p300 peptide site for lysine presented in the KXXK sequence motif [10, 11]. The methyl-urea of A-485 is inserted through the L1 loop where it makes two equivalent hydrogen bonds to Gln-1455 (Fig. 2b). Two other notable hydrogen bonds are made between the 4' carbonyl of the oxazolidinedione to Ser-1400 and from the amide carbonyl to a coordinated water molecule. The majority of the remaining molecular interactions are hydrophobic in nature including the fluorophenyl ring which sits in a hydrophobic pocket that expands by means of a shift in helix 3 to accommodate its size (Fig. 2c). Consistent with its lack of activity, the urea moiety of A-486 would be expected to clash with Gln-1455 and Lys-1456 on the side of the L1 loop. Since substantial sequence divergence between HATs has been reported [12], we further utilized the structure to gain insight into the selectivity of A-485 for p300/CBP over other HATs. As shown in Extended Data Fig. 4a, the specificity of A-485 likely stems primarily from the L1 loop which is absent in other HATs. Superposition of the HAT domains of hPCAF, hMYST3, hHAT1, hTIP60 and hGCN5 with A-485 reveals that each would be predicted to clash with A-485, making it unlikely that other HAT family members would be able to make the necessary structural accommodations to provide potent binding. For example, the indane ring of A-485 would interfere with the alpha backbone of the motif A helix of PCAF (Extended Data Fig. 4b). These structural superpositions are consistent with the HAT inhibitor specificity that we

observe for A-485 (Supplementary Table 3). The activity assay IC_{50} for inhibition increased linearly with increasing concentrations of acetyl-CoA (Fig. 2d) confirming acetyl-CoA competitive inhibition. An AlphaLISA-based peptide substrate binding assay demonstrated that unlabeled peptide but not A-485 competed with binding, confirming that A-485 is not competitive with the peptide substrate (Extended Data Fig. 4c). Together, these results indicate that A-485 is an acetyl-CoA competitive catalytic inhibitor of p300/CBP.

Prior genetic studies indicate that p300/CBP preferentially acetylates H3K18/K27 but not H3K9 [13]. As shown in Fig. 3a via a high content microscopy-based assay [14], A-485 treatment (3 h) of prostate adenocarcinoma PC-3 cells resulted in a dose dependent decrease of H3K27Ac (EC_{50} = 73 nM) but not H3K9Ac (EC_{50} > 10,000 nM). A-486 was inactive (Fig. 3a), and only modest inhibition was observed upon C646 treatment (Extended Data Fig. 5a). Inhibition of H3K18Ac similar to that of H3K27Ac was also observed (Supplementary Table 8), and inhibition of both p300/CBP acetylation sites was sustained at 24 h in multiple cell lines. To broadly assess cellular selectively of A-485, we evaluated an array of H3 and H4 epigenetics marks [14]. We confirmed A-485 only inhibited H3K27Ac and H3K18Ac while A-486 was inactive, indicating that A-485 was selective for p300/CBP over other HATs and histone methyltransferases (HMTs) in cells (Fig. 3b and Extended Data Fig. 5b). Similar results were observed using western blotting (Extended Data Fig. 5c). In addition to histone substrates, we further confirmed by mass spectrometry analysis that A-485 caused a marked decrease of multiple acetylation sites found within the p300/CBP activation loop (Supplementary Table 9) [11]. Inhibition of K1499Ac/K1535Ac of p300/CBP was further confirmed by site specific antibodies via western blotting (Extended Data Fig. 5d). A-485 treatment did not alter p300 or CBP protein levels (Extended Data Fig. 5e).

Since p300 and CBP are involved in the development and progression of multiple human malignancies [15, 16, 17], we evaluated the ability of A-485 to inhibit proliferation across 124 cancer cell lines encompassing diverse lineages. (Fig. 3c, Supplementary Table 10). The broadest sensitivity was observed in hematological tumors, where A-485 exhibited potent activity in most multiple myeloma (MM) cell lines, a subset of acute myeloid leukemia (AML) lines and non-Hodgkin's lymphoma (NHL) lines. In contrast, multiple solid tumor lines including melanoma, small cell lung cancer (SCLC), and triple negative breast cancer (TNBC) were significantly less sensitive to A-485. Interestingly, we observed potent inhibition of proliferation by A-485 in AR^+, but not AR^- prostate cancer cell lines [18] (Extended Data Fig. 5f). To validate these results, we knocked down p300/CBP via siRNA and confirmed growth inhibition of AR^+ LnCaP-FGC cells and inhibition of H3K18Ac and H3K27Ac but not H3K9Ac (Extended Data Fig. 6). However, despite the differential proliferation sensitivity, A-485 induced a similar decrease of H3K27Ac in all 5 prostate cancer cell lines. These results indicate that A-485 selectively inhibits hematological and prostate cancer cell proliferation and that inhibition of p300/CBP-mediated global histone acetylation does not necessarily translate to an anti-proliferative phenotype.

Since p300 is a key co-activator of AR activity [17, 19] and is up-regulated during prostate cancer progression [16, 20], we evaluated whether A-485 modulated AR transcriptional activity. Treatment of the androgen dependent LnCaP-FGC cell line with A-485, but not A-486, attenuated DHT-stimulated PSA expression more potently than the AR antagonist

enzalutamide (Fig. 4a). This inhibition was observed at both early (7 h) and later (24 h) time points, suggesting direct inhibition of AR transcriptional activity. Additional AR-dependent genes TMPRSS2 and SLC45A3 were inhibited by A-485 (Extended Data Fig. 7a). A-485 also further inhibited AR beyond the basal activity observed upon androgen deprivation (Extended Data Fig. 7b). Similar results were observed in VCaP cells, another androgen-dependent prostate adenocarcinoma cell line (Extended Data Fig. 7c,d). These gene expression changes resulted in dose-dependent reduction of protein levels, where A-485 inhibited the induction of PSA upon DHT stimulation and further reduced basal PSA expression upon androgen depletion (Extended Data Fig. 7e).

Since A-485 does not act as an AR antagonist (Extended Data Fig. 8a), we evaluated the effects of A-485 on H3K27Ac deposition and AR occupancy at the PSA enhancer via chromatin immunoprecipitation (ChIP). DHT stimulation of LnCaP-FGC cells for 6 h induced an increase in H3K27Ac deposition (Fig. 4b) and AR binding (Fig. 4c) at the androgen response element (ARE) of the PSA enhancer. Treatment with A-485 and enzalutamide both reduced H3K27Ac binding (Fig. 4b), but only enzalutamide decreased AR occupancy (Fig. 4c), suggesting that p300/CBP is important for AR trans-activation but not AR complex formation. Given that p300 regulates AR activity downstream of ligand binding, 22Rv1 cells that are AR dependent but proliferate in the absence of androgens and express AR splice variants (AR-SVs) should still respond to p300/CBP inhibition. Indeed, A-485 inhibited proliferation in the absence of androgens and decreased PSA expression at early (7 h) and late (24 h) time points in this model while A-486 and enzalutamide were inactive (Extended Data Fig. 8b,c).

To evaluate AR-dependent global transcription changes, we performed gene expression profiling (Fig. 4d). In LnCaP-FGC cells, analysis of 217 genes that were modulated by DHT indicated that A-485 antagonized expression of the up-regulated genes in an almost identical pattern to enzalutamide after 6 h. However, in contrast to enzalutamide, A-485 did not reverse the expression of a subset of genes that were repressed by DHT treatment, establishing that p300 acts as an AR co-activator. A-485 also induced down-regulation of 40% of these same DHT responsive genes in androgen depleted 22Rv1 cells (Fig. 4d) and similar to the LnCaP-FGC cells did not modulate the DHT-repressed genes. In contrast, enzalutamide was inactive in these cells (Fig. 4d). We also assessed the global changes of gene expression upon A-485 treatment at this early time, where regulation of gene expression was likely to be direct. At both low and high concentrations, A-485 conferred predominantly gene down-regulation, providing further evidence that p300/CBP acts primarily to positively regulate gene expression (Supplementary Table 11). Further analysis utilizing the Ingenuity upstream regulator analysis indicated that both enzalutamide and A-485 inhibited hormone signaling pathways as expected in LnCaP-FGC cells but only A-485 induced robust inhibition in multiple other signaling pathways and transcriptional regulators including c-Myc (Extended Data Fig. 9). c-Myc is strongly correlated with prostate cancer progression [21], is an important p300 target in CBP-deficient cancers [22], and is a key oncogenic transcription factor that is regulated by superenhancer regions containing p300/CBP and identified by high density of H3K27Ac [23]. Indeed, A-485 robustly decreased c-Myc expression while enzalutamide had no effect (Fig. 4e, Extended Data Fig. 10a).

Since A-485 treatment inhibited the proliferation and AR dependent transcription of castration resistant prostate cancer cells and displayed favorable ADME properties and PK profile (Fig. 1a and Supplementary Table 12), we evaluated whether A-485 could inhibit tumor growth *in vivo* using an AR positive, patient derived castration resistant prostate cancer model, the LuCaP-77 CR xenograft model. After tumors were established in SCID male mice, twice daily intraperitoneal injections of A-485 induced 54% tumor growth inhibition (TGI) after 21 days of dosing ($p<0.005$ as compared to vehicle control, Fig. 4f). In addition, dosing A-485 in tumor-bearing animals for 7 days induced a decrease in the mRNA levels of AR-dependent gene SLC45A3 and c-Myc at 3 h post-dosing and translated for c-Myc to the protein level (Extended Data Fig. 10b,c), indicating that A-485 inhibited p300-mediated transcriptional activity *in vivo*. However, at 16 h post-dosing on day 7, A-485 drug levels in the plasma and tumor decreased as compared to 3 h (Extended Data Fig. 10d). Concomitant to this, expression of SLC45A3 and c-Myc rebounded to pre-treatment levels, indicating that A-485 did not inhibit these markers at Ctrough levels under the BID dosing regimen employed. A-485 induced a moderate 9% body weight loss, and the animals rapidly recovered upon completion of the A-485 dosing regimen (Extended Data Fig. 10e).

In summary, we have overcome the long-standing challenge of developing a drug-like HAT inhibitor by identifying a first-in-class highly potent, selective, cell and *in vivo* active p300/CBP catalytic inhibitor, A-485. A similar approach also can be applied more broadly to develop inhibitors of other HATs. Furthermore, they underscore the value of therapeutically targeting the HAT activity of p300/CBP, providing a major advance in the road to evaluating the clinical utility of HAT inhibitors for multiple human diseases.

Extended Data

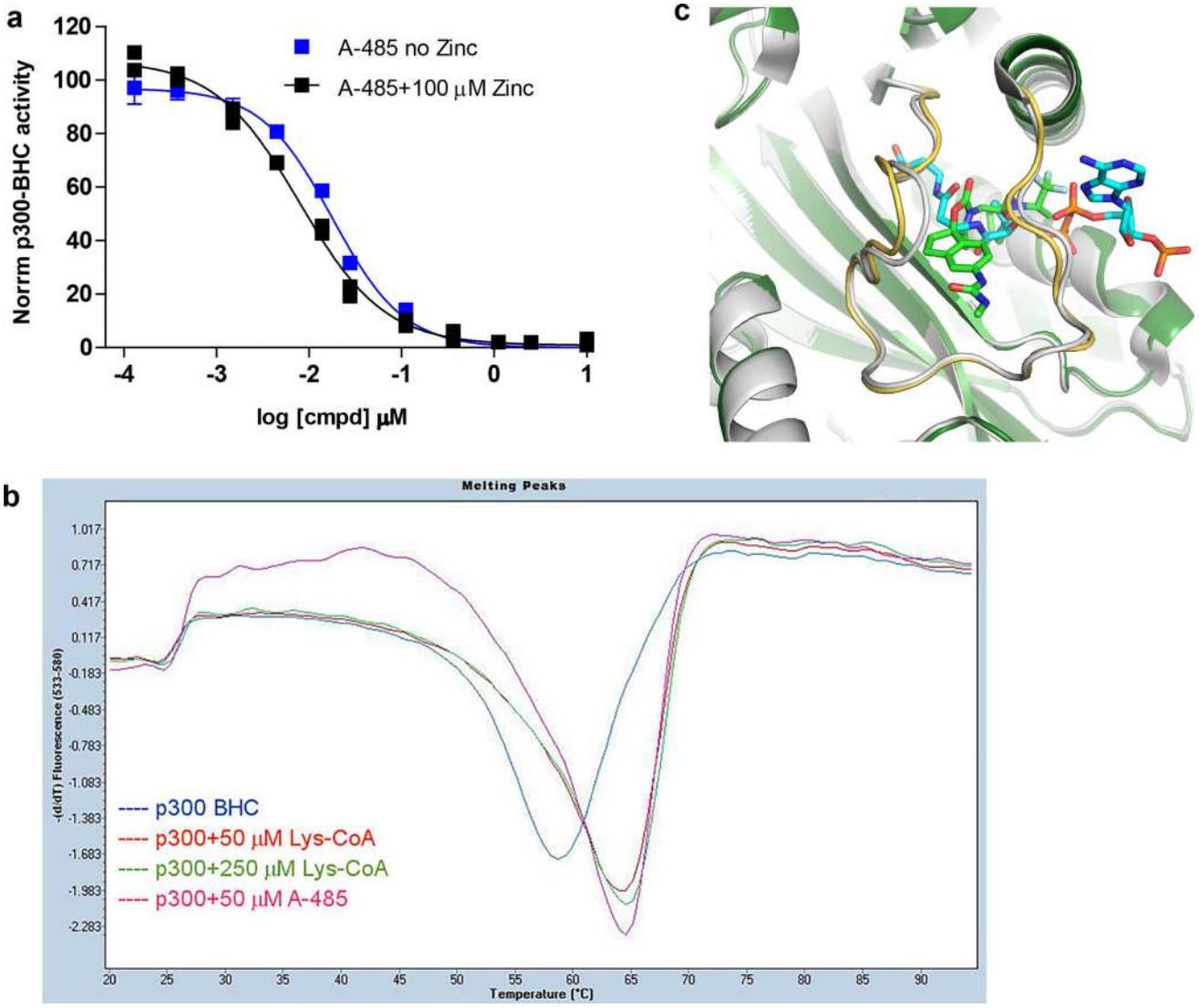

Extended Data Figure 1. A-485 binds to p300-BHC

(a) A-485 inhibits the acetyltransferase activities of p300-BHC under EDTA-free conditions. The TR-FRET activity assay was performed using p300-BHC purified in the absence of EDTA and without EDTA in the assay buffer. The TR-FRET signal observed with DMSO control was normalized to 100. Error bars represent the S.D. of 3 independent biological replicates (A-485 no Zinc); n=2 for A-485+100 μM Zinc. Source data for (a) is provided. (b) A-485 binding to p300-BHC was assessed via a thermal shift assay (TSA) as described in the Online Methods. Lys-CoA was used a positive control. A-485 and both concentrations of Lys-CoA increased the stability of p300-BHC by 5.8 °C. A representative melting profile of four independent experiments is shown. (c) Superposition of the Δp300 HAT A-485 complex (green) with the inactive Δp300 HAT Y1467F mutant (white) complexed with acetyl-CoA (teal) (PDB ID: 4PZS) shows A-485 is competitive with acetyl-CoA. The L1 loop is shown in yellow.

	A-485 (5KJ2)
Data collection	
Space group	$C222_1$
Cell dimensions	
a, *b*, *c* (Å)	45.19, 102.94, 168.44
α, β, γ (°)	90.00, 90.00, 90.00
Resolution (Å)	1.95(1.953-1.947)[a]
R_{merge}	0.058 (0.870)
$I/\sigma(I)$	20.3 (2.2)
Completeness (%)	100.0 (100.0)
Redundancy	6.6 (6.9)
Refinement	
Resolution (Å)	84.22-1.95
No. reflections	29345
R_{work} / R_{free}	0.225/0.260
No. atoms	2884
Protein	2586
A-485/Na	38/1
Water	259
B factors	
Protein	39.3
A-485/Na	39.6/24.3
Water	44.7
R.m.s. deviations	
Bond lengths (Å)	0.010
Bond angles (°)	1.11

[a] Values in parentheses are for highest-resolution shell. Data was obtained from a single crystal.

Extended Data Figure 2. Data collection and refinement statistics for Δp300 HAT Domain complexed with A-485

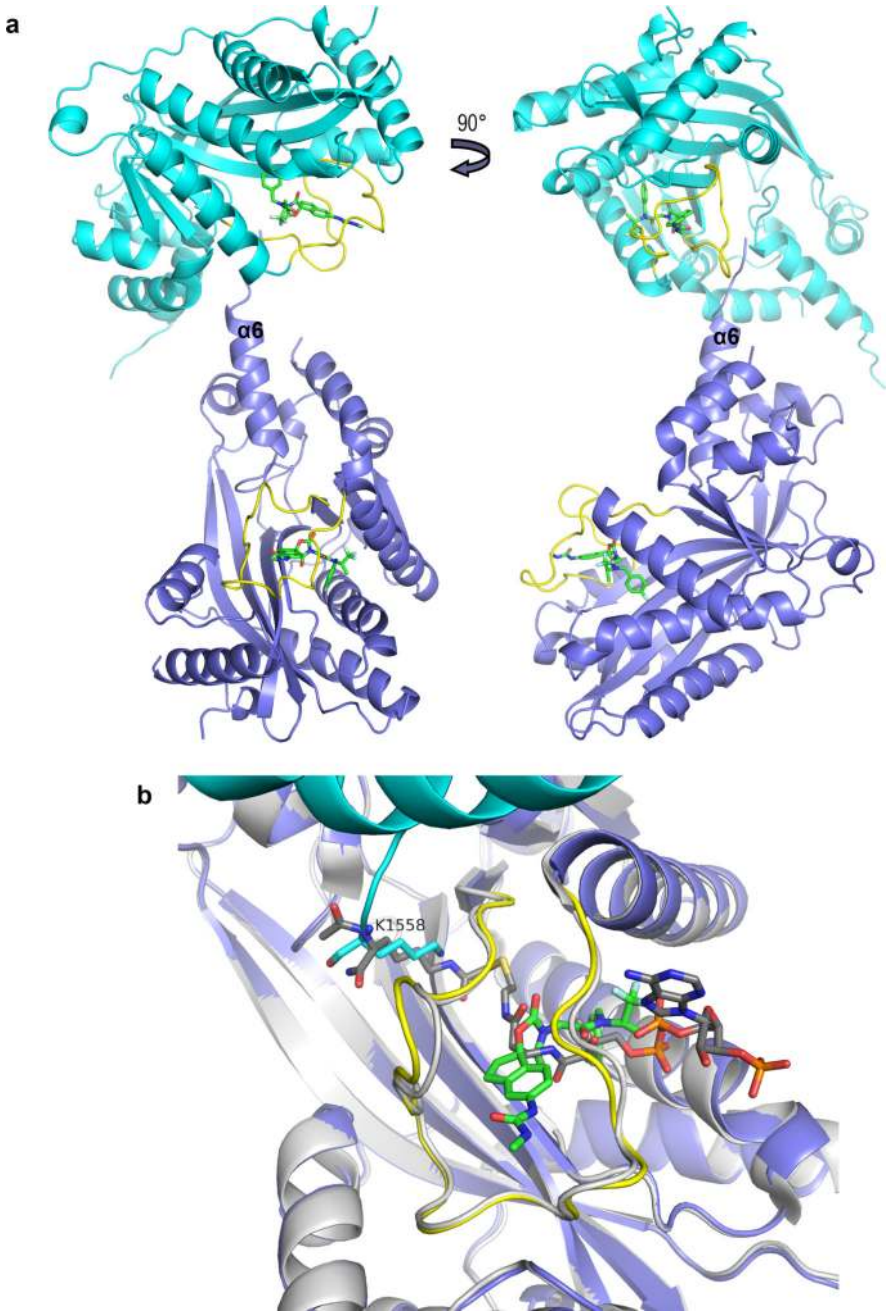

Extended Data Figure 3. Δp300 HAT-A-485 complex crystal packing with lysine tunnel insertion
(a) The loop at the end of helix 6 inserts into the peptide binding site of a symmetry related molecule (teal). A-485 is shown in green sticks, and the L1 loop is yellow. (b) Lys-1558 of a symmetry related Δp300 HAT (teal) inserts into the lysine tunnel in a similar fashion as the lysine portion of Lys-CoA (PDB ID: 3BIY) (gray) bound in the inactive Δp300 HAT Y1467F mutant (PDB ID: 3BIY).

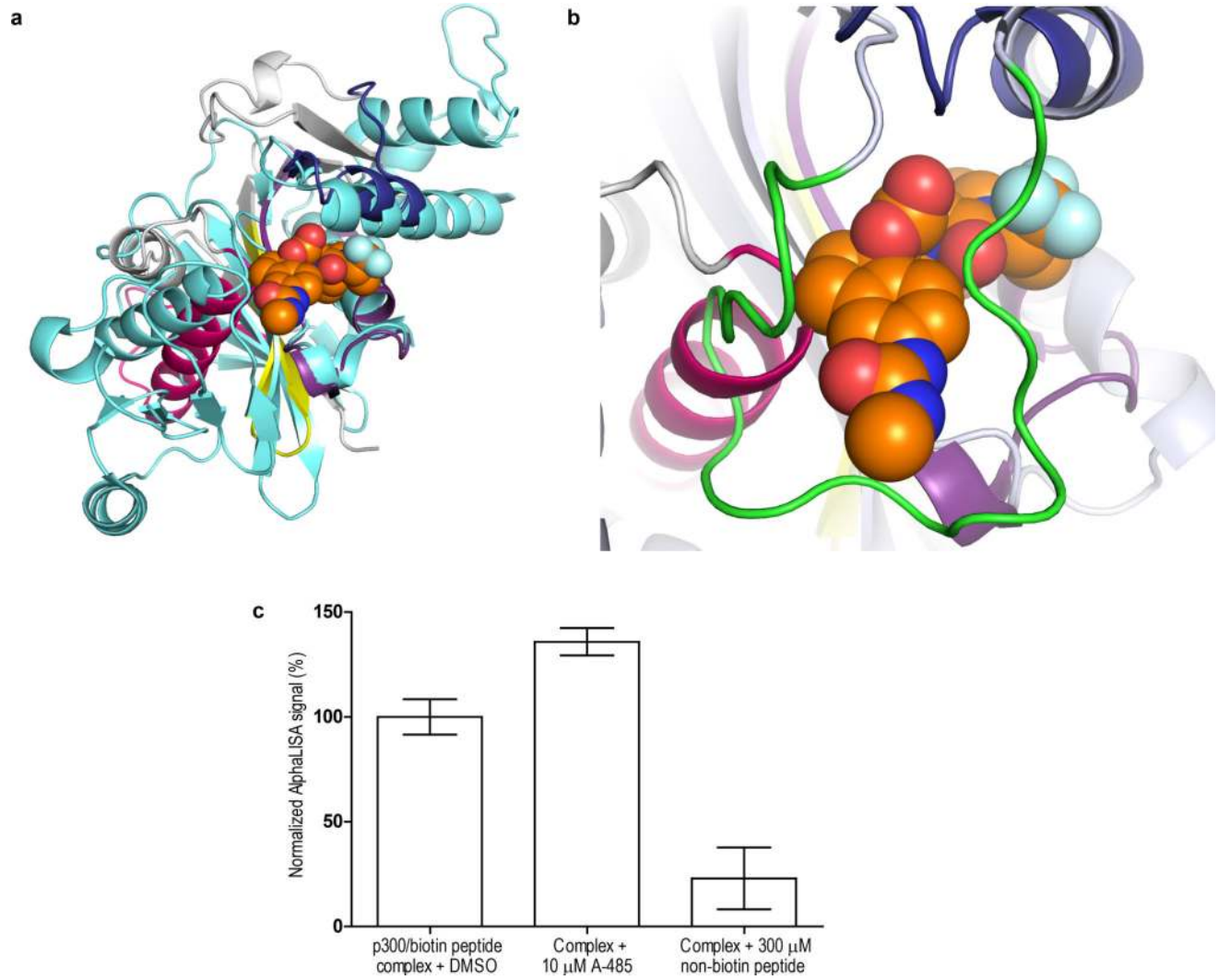

Extended Data Figure 4. Structural model of specificity of A-485 for p300/CBP over other HATs

(a) Superposition of human PCAF (PDB ID: 1CM0) in white showing motifs A-D colored magenta, yellow, purple, and blue respectively with human TIP60 (PDB ID: 2OU2) in cyan, and A-485 in orange spheres. These two HATs serve as representatives of the two primary structural classes observed upon superposition of the HAT domains of hMYST3 (PDB ID: 2OZU), hPCAF (PDB ID: 1CM0), hHAT1 (PDB ID: 2P0W), hTIP60 (PDB ID: 2OU2), and hGCN5 (PDB ID: 1Z4R). (b) Zoomed in view of superposition of human PCAF as above and of p300 in pale blue complexed with A-485 with the L1 loop shown in green. Note that both the L1 loop and A-485 clash with the Helix in motif A. (c) A-485 does not compete with peptide substrate binding to p300-BHC protein. Peptide binding was assessed via an AlphaLISA-based peptide substrate binding assay as described in the Online Methods. All data were normalized to the p300-BHC/biotin peptide complex signal set at 100%. All measurements are the result of 29 technical replicates over two independent experiments. Error bars represent S.D. of the technical replicates.

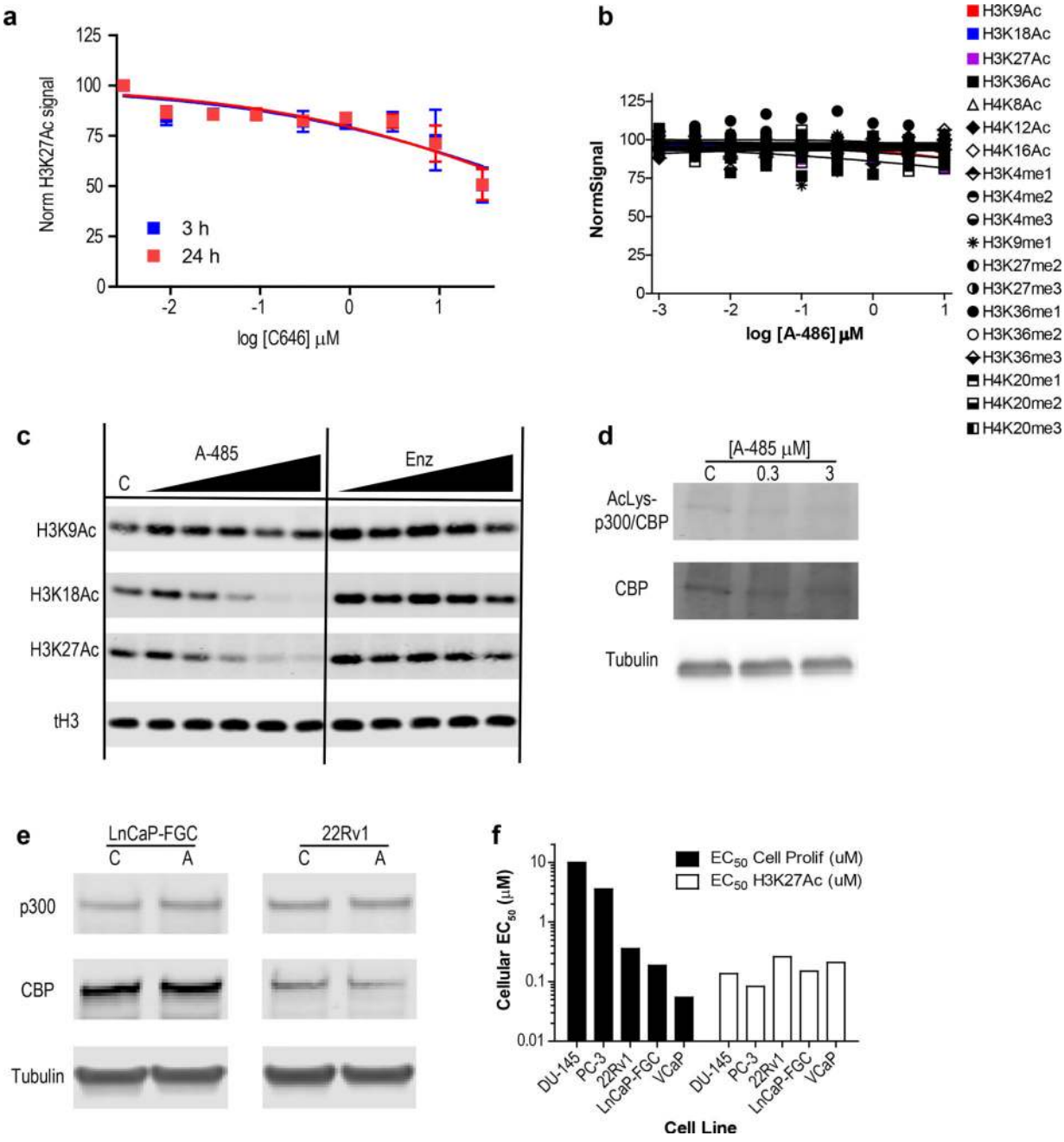

Extended Data Figure 5. A-485 is more potent than C646 and decreases p300/CBP auto-acetylation in cells

(a) PC-3 cells were treated with C646 for the indicated times and then processed for H3K27Ac via high content microscopy as described in the Online Methods. The fluorescent intensity observed with the DMSO control for H3K27Ac was normalized to 100. Error bars represent the S.D. of 4 independent biological replicates. (b) PC-3 cells were treated with A-486 for 3 h and then processed for high content microscopy as described in the Online Methods (n=2). Source data for (a,b) are provided. (c) A-485 but not enzalutamide (Enz) inhibits H3K27Ac and H3K18Ac in DHT-stimulated LnCaP-FGC cells after 24 h. Cells were treated with 5-fold dilutions of A-485 or enzalutamide (Enz) starting at 10 μM or

DMSO as a control (C). A representative western blot of 2 independent biological replicates is shown. (d) 22Rv1 cells were treated with 0.3 μM or 3 μM A-485 or DMSO as a control (C) for 1 h and processed for western blotting as described in the Online Methods. (e) Cells were treated with 3 μM A-485 (A) or DMSO as a control (C) for 24 h and processed for western blotting as described in the Online Methods. (f) A-485 exhibits similar inhibition of H3K27Ac in AR^+ and AR^- prostate cancer cells (experiment performed as per Fig. 3a) but is selectively anti-proliferative in AR^+ cells (data from Fig. 3c is shown). For (c-e) gel source data, see Supplementary Figure 1

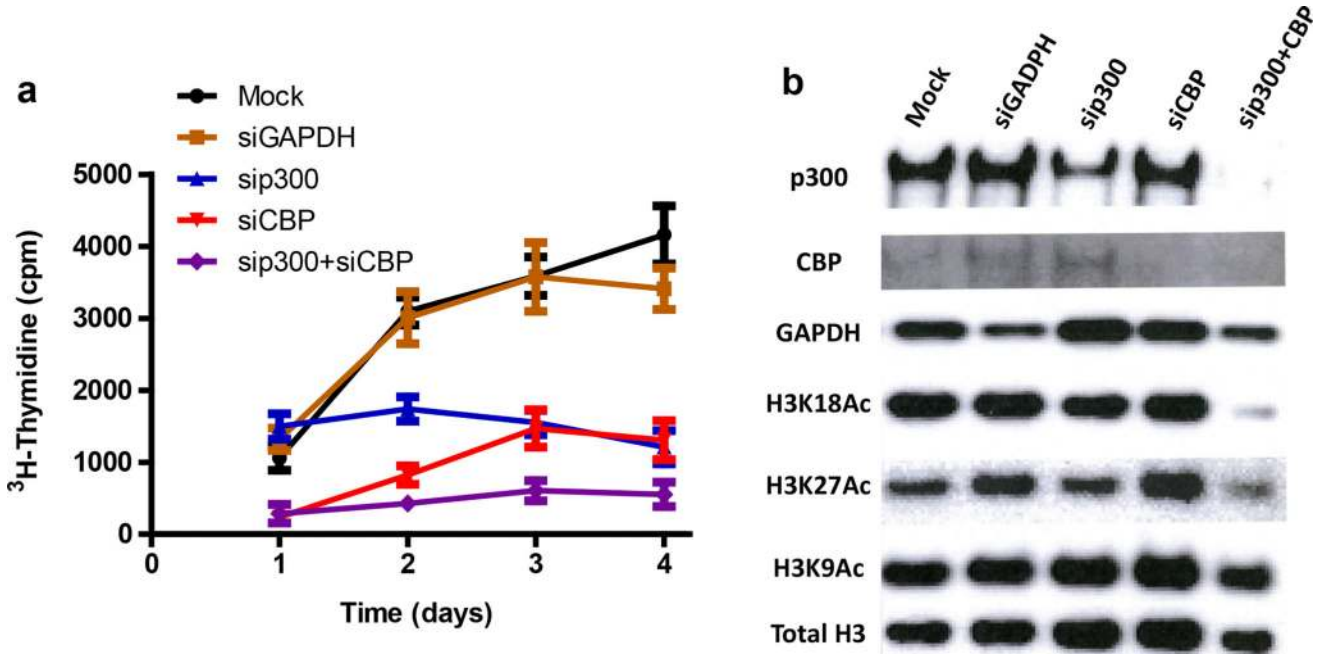

Extended Data Figure 6. p300/CBP siRNAs inhibit cell proliferation and p300/CBP activity in LnCaP-FGC cells

LnCaP-FGC cells were starved of androgens for 72 h and then the indicated siRNAs were delivered via nucleofection. After 24 h, cells were then treated with 30 pM Mibolerone and either (a) measured at indicated times for ^{3}H-Thymidine incorporation or (b) processed at 2 days for western blotting for the indicated proteins as described in the Online Methods. Error bars represent the S.D. of 8 technical replicates. Source data for (a) is provided. For gel source data, see Supplementary Figure 1

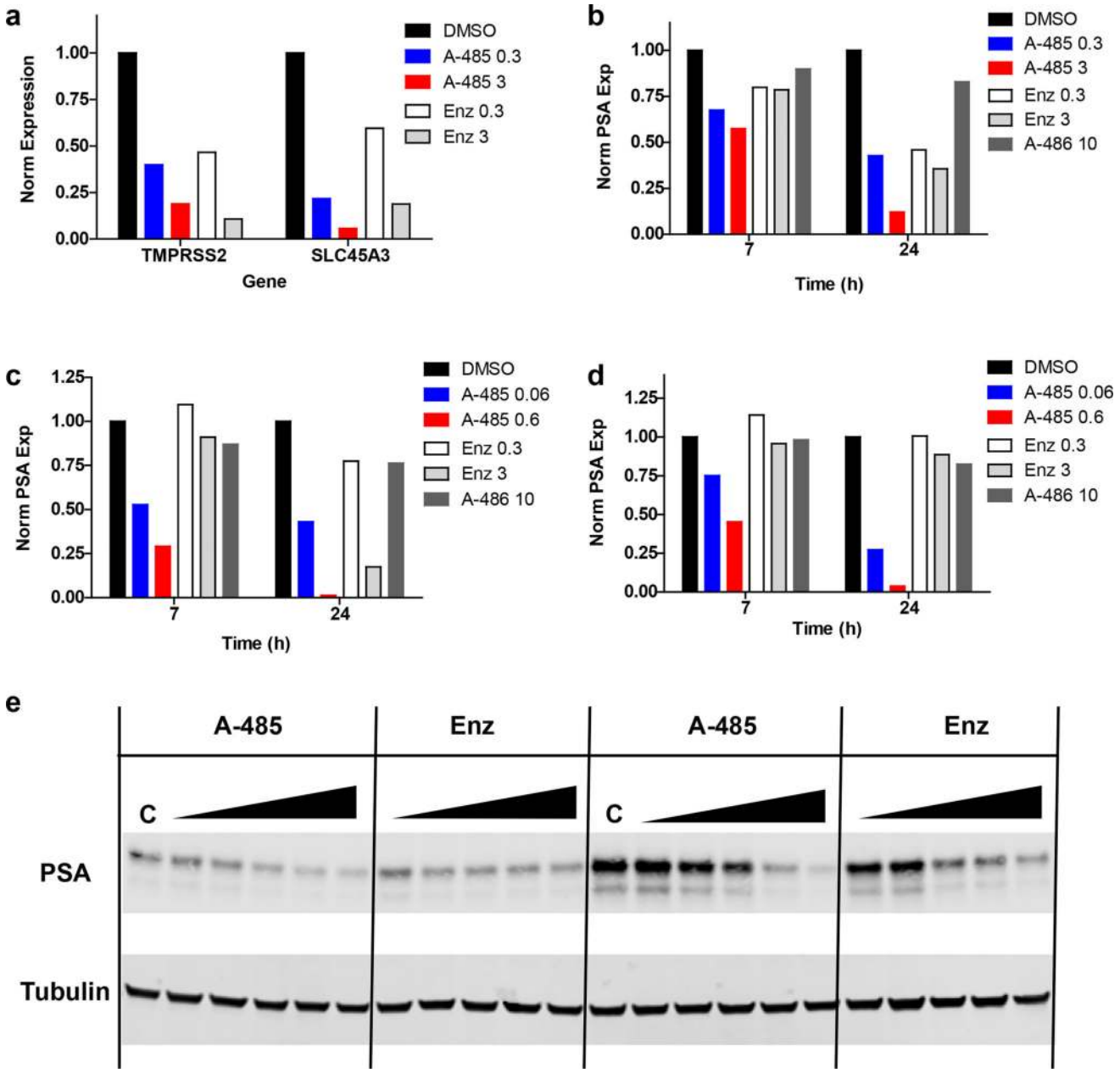

Extended Data Figure 7. A-485 inhibits AR activity in LnCaP-FGC and VCaP cells

DHT-stimulated (a) or androgen depleted (b) LnCaP-FGC cells were treated with the indicated compounds at the indicated concentrations (in μM) for 24 h and processed for qRT-PCR for the indicated genes as described in the Online Methods. (c,d) VCaP cells were starved of androgens for 24 h and then treated as per (a,b). The mean of n=2 independent experiments is shown for (a-d). The expression (Exp) observed for the DMSO control of in the indicated genes was normalized to 1 using the Bio-Rad CFX 3.1 Manager software. Source data for (a-d) are provided. (e) LnCaP-FGC cells were treated with compounds as per Extended Data Fig. 5c and processed for western blotting as described in the Online Methods. For gel source data, see Supplementary Figure 1.

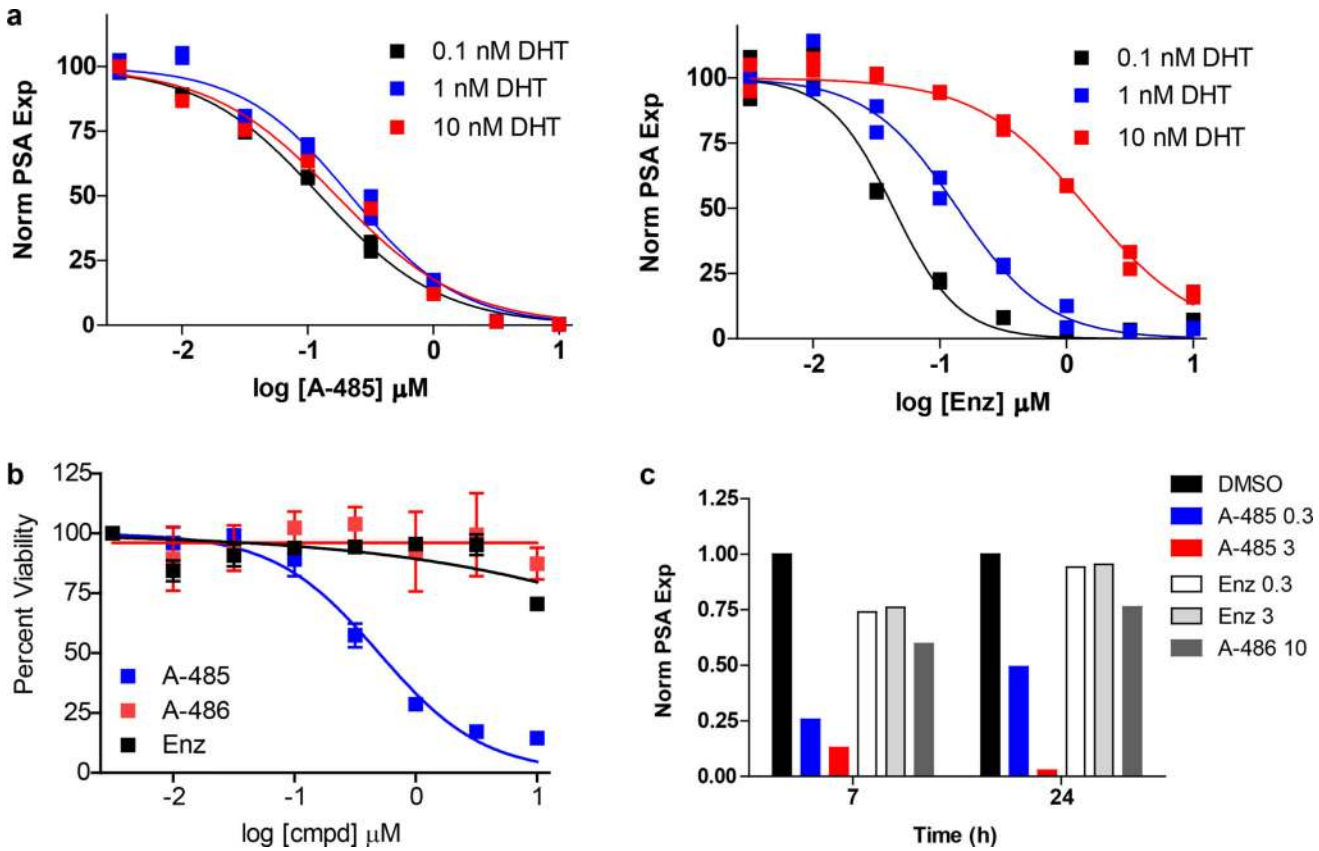

Extended Data Figure 8. A-485 inhibits AR activity in a manner distinct from AR antagonism and inhibits proliferation and PSA expression in 22Rv1 cells

(a) DHT-stimulated LnCaP-FGC cells were treated with A-485 (left panel) or Enz (right panel) for 24 h and processed for qRT-PCR analysis as described in the Online Methods. Enz is shown as an AR antagonist control. (b) Androgen depleted 22Rv1 cells were treated with the indicated compounds for 5 days and processed for analysis of cell proliferation as described in the Online Methods. Error bars represent the S.D. of 6 independent experiments for A-485 and 3 independent experiments for A-486 and Enz. (c) 22Rv1 cells were starved of androgens for 72 h and then treated with the indicated compounds for 24 h and processed for qRT-PCR as described in the Online Methods. The mean of n=2 independent experiments is shown for (a,c). The PSA expression (Exp) observed for the DMSO control was normalized to 1 using the Bio-Rad CFX 3.1 Manager software. Source data for (a-c) are provided.

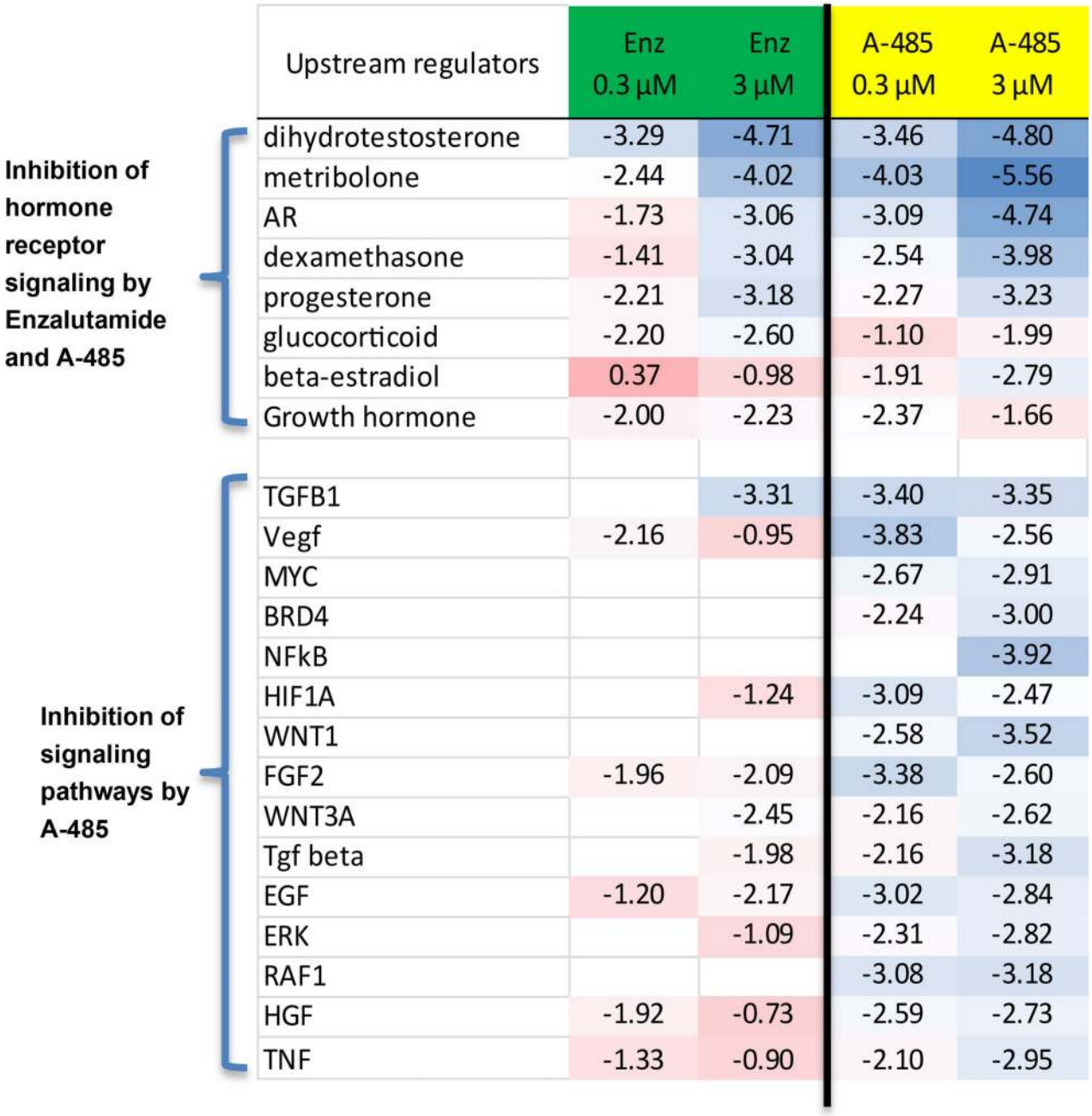

	Upstream regulators	Enz 0.3 µM	Enz 3 µM	A-485 0.3 µM	A-485 3 µM
Inhibition of hormone receptor signaling by Enzalutamide and A-485	dihydrotestosterone	-3.29	-4.71	-3.46	-4.80
	metribolone	-2.44	-4.02	-4.03	-5.56
	AR	-1.73	-3.06	-3.09	-4.74
	dexamethasone	-1.41	-3.04	-2.54	-3.98
	progesterone	-2.21	-3.18	-2.27	-3.23
	glucocorticoid	-2.20	-2.60	-1.10	-1.99
	beta-estradiol	0.37	-0.98	-1.91	-2.79
	Growth hormone	-2.00	-2.23	-2.37	-1.66
Inhibition of signaling pathways by A-485	TGFB1		-3.31	-3.40	-3.35
	Vegf	-2.16	-0.95	-3.83	-2.56
	MYC			-2.67	-2.91
	BRD4			-2.24	-3.00
	NFkB				-3.92
	HIF1A		-1.24	-3.09	-2.47
	WNT1			-2.58	-3.52
	FGF2	-1.96	-2.09	-3.38	-2.60
	WNT3A		-2.45	-2.16	-2.62
	Tgf beta		-1.98	-2.16	-3.18
	EGF	-1.20	-2.17	-3.02	-2.84
	ERK		-1.09	-2.31	-2.82
	RAF1			-3.08	-3.18
	HGF	-1.92	-0.73	-2.59	-2.73
	TNF	-1.33	-0.90	-2.10	-2.95

Extended Data Figure 9. Ingenuity upstream regulator analysis indicates that A-485 but not Enz inhibits additional pathways beyond hormone receptor at 6 h

Z-scores of >2 and <-2 are significant.

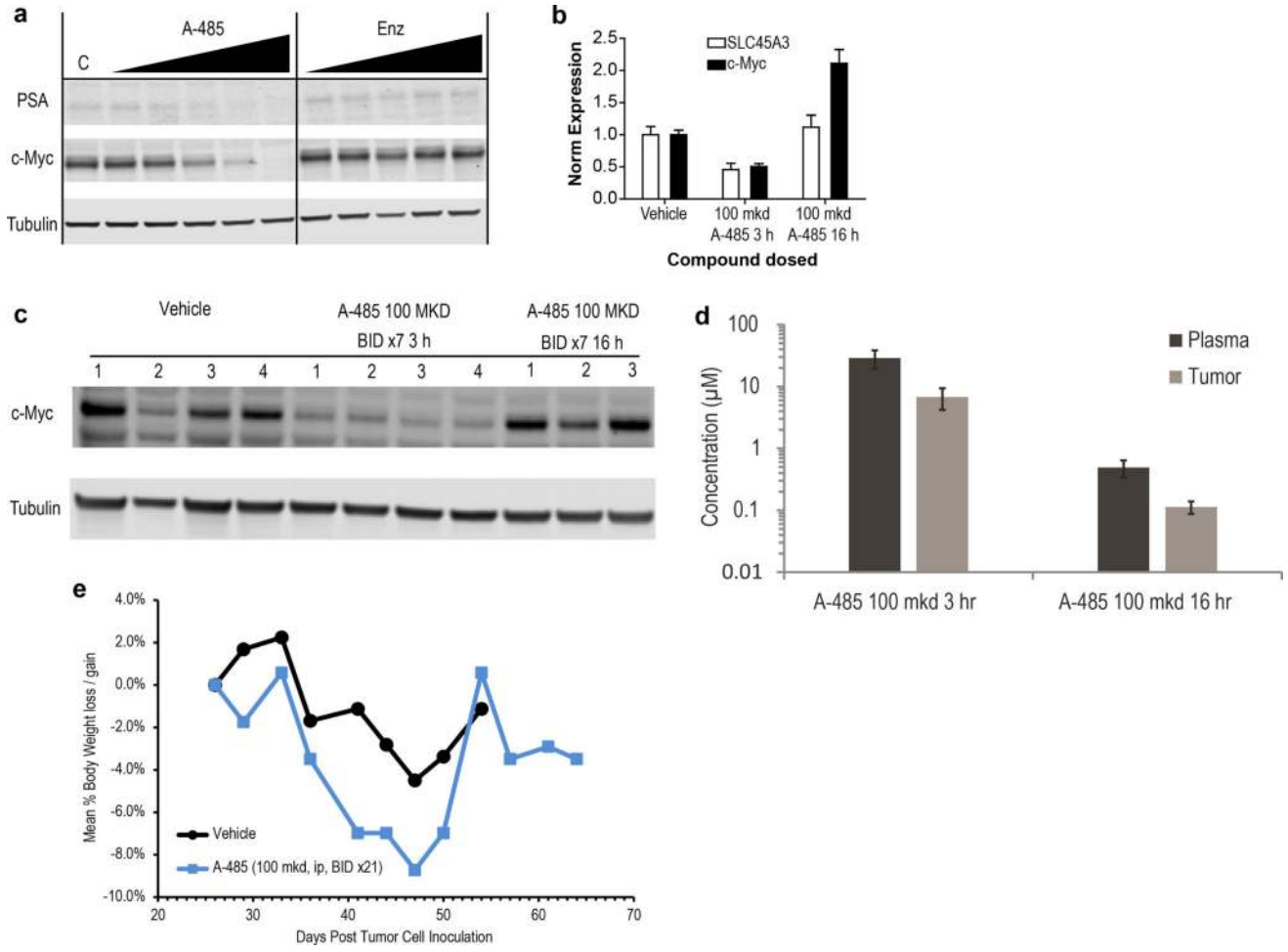

Extended Data Figure 10. A-485 inhibits c-Myc in 22Rv1 cells and A-485 dosing of LuCaP-77 CR tumor bearing mice tumor induces a decrease in tumor c-Myc protein levels and moderate body weight loss

(a) Androgen-depleted 22Rv1 cells were treated with A-485 or Enz for 24 h and processed for western blot analysis as described in the Online Methods. A representative western blot of 2 independent biological replicates is shown. (b) A-485 dosing of LuCaP-77 CR tumor bearing mice induces a decrease in tumor SLC45A3 and c-Myc mRNA levels. Animals were dosed for 7 days per the BID dosing schedule shown in Fig. 4f and tumors were excised 3 h and 16 h post final dose. Expression (Exp) in (b) was normalized as per Fig. 4a. Error bars represent the S.D. of n=4 animals per indicated group. (c) LuCap-77 CR tumor-bearing mice were dosed with the A-485 or vehicle control as per (b) and tumors were processed for western blot analysis as described in the Online Methods. For (a,c) gel source data, see Supplementary Figure 1. (d) Exposure of A-485 in plasma and tumors after 7 d dosing of A-485. Error bars represent the S.D. of 4 animals. (e) Average body weight for same animals bearing LuCaP-77 CR tumors dosed with A-485 in Fig. 4f. The mean body weights of the animals (n=8) in each group were measured. Source data for (b,d, and e) are provided.

Supplementary Material

Refer to Web version on PubMed Central for supplementary material.

Acknowledgments

We thank Vivek Abraham and Morey Smith for high content microscopy assistance and Scott Ackler, David He, Ziping Yang, and Ricky Bellin for assistance with cell proliferation assays. We thank Hong Liu for assistance with pharmacokinetic analyses, Gilbert Diaz with compound selectivity screening, and Rodger Henry for compound x-ray crystallography assistance. We thank Eva Corey for the LuCap-77 CR patient derived xenograft model. HAT selectivity, 7TM, and ion channel off-target selectivity screening was supplied by Eurofins-Cerep. Use of the IMCA-CAT beamline 17-ID at the Advanced Photon Source was supported by the companies of the Industrial Macromolecular Crystallography Association through a contract with Hauptman-Woodward Medical Research Institute. Use of the Advanced Photon Source was supported by the U.S. Department of Energy, Office of Science, Office of Basic Energy Sciences, under Contract No. DE-AC02-06CH11357. C.C. is supported by the Hallas Møller Investigator award from the Novo Nordisk Foundation (NNF14OC0008541). The Novo Nordisk Foundation Center for Protein Research is supported financially by the Novo Nordisk Foundation (Grant agreement NNF14CC0001). P.A.C. was supported by the NIH and FAMRI foundation.

Competing financial Interests

This study was sponsored by AbbVie. AbbVie contributed to the study design, research, and interpretation of data, writing, reviewing, and approving the publication. L.M.L, C.G.J., R.P.E, W.Q., D.M., E.D., T.M.H, R.R, R.F., V.M., B.S., M.A., P.H., L.L., T.U., E.F., D.F., F.G.B., M.T., G.G.C., C.S., M.R.M., S.R., A.L., and K.D.B. were employees of AbbVie at the time of the study. K.K., J.W.L., P.D.V., D.M., E.K. were employees of Acylin which provided assets to AbbVie at the time of the study. AbbVie licensed and provided funding for these assets. R.M. and P.A.C. are co-founders of Acylin and consultants for Abbvie.

References

1. Tessarz P, Kouzarides T. Histone core modifications regulating nucleosome structure and dynamics. Nat. Rev. Mol. Cell. Biol. 2014; 15:703–708. [PubMed: 25315270]
2. Simon RP, Robaa D, Alhalabi Z, Sippl W, Jung M. KATching-Up on Small Molecule Modulators of Lysine Acetyltransferases. J. Med. Chem. 2016; 59:1249–1270. [PubMed: 26701186]
3. Iyer NG, Ozdag H, Caldas C. p300/CBP and cancer. Oncogene. 2004; 23:4225–4231. [PubMed: 15156177]
4. Balasubramanyam K, et al. Polyisoprenylated benzophenone, garcinol, a natural histone acetyltransferase inhibitor, represses chromatin transcription and alters global gene expression. J. Biol. Chem. 2004; 279:33716–33726. [PubMed: 15155757]
5. Lau OD, et al. HATs off: selective synthetic inhibitors of the histone acetyltransferases p300 and PCAF. Mol. Cell. 2000; 5:589–595. [PubMed: 10882143]
6. Bowers EM, et al. Virtual ligand screening of the p300/CBP histone acetyltransferase: identification of a selective small molecule inhibitor. Chem. Biol. 2010; 17:471–482. [PubMed: 20534345]
7. Shrimp JH, et al. Characterizing the Covalent Targets of a Small Molecule Inhibitor of the Lysine Acetyltransferase P300. ACS Med. Chem. Lett. 2016; 7:151–155. [PubMed: 26985290]
8. Lopes da Rosa J, Bajaj V, Spoonamore J, Kaufman PD. A small molecule inhibitor of fungal histone acetyltransferase Rtt109. Bioorg. Med. Chem. Lett. 2013; 23:2853–2859. [PubMed: 23587423]
9. Maksimoska J, Segura-Pena D, Cole PA, Marmorstein R. Structure of the p300 histone acetyltransferase bound to acetyl-coenzyme A and its analogues. Biochemistry. 2014; 53:3415–3422. [PubMed: 24819397]
10. Liu X, et al. The structural basis of protein acetylation by the p300/CBP transcriptional coactivator. Nature. 2008; 451:846–850. [PubMed: 18273021]
11. Thompson PR, et al. Regulation of the p300 HAT domain via a novel activation loop. Nat. Struct. Mol. Biol. 2004; 11:308–315. [PubMed: 15004546]
12. Marmorstein R. Structure of histone acetyltransferases. J. Mol. Biol. 2001; 311:433–444. [PubMed: 11492997]

13. Jin Q, et al. Distinct roles of GCN5/PCAF-mediated H3K9ac and CBP/p300-mediated H3K18/27ac in nuclear receptor transactivation. EMBO J. 2011; 30:249–262. [PubMed: 21131905]
14. Bromberg KD, et al. The SUV4-20 inhibitor A-196 verifies a role for epigenetics in genomic integrity. Nat. Chem. Biol. 2017; 13:317–324. [PubMed: 28114273]
15. Wang L, et al. The leukemogenicity of AML1-ETO is dependent on site-specific lysine acetylation. Science. 2011; 333:765–769. [PubMed: 21764752]
16. Debes JD, et al. p300 in prostate cancer proliferation and progression. Cancer Res. 2003; 63:7638–7640. [PubMed: 14633682]
17. Zhong J, et al. p300 acetyltransferase regulates androgen receptor degradation and PTEN-deficient prostate tumorigenesis. Cancer Res. 2014; 74:1870–1880. [PubMed: 24480624]
18. Santer FR, et al. Inhibition of the acetyltransferases p300 and CBP reveals a targetable function for p300 in the survival and invasion pathways of prostate cancer cell lines. Mol. Cancer Ther. 2011; 10:1644–1655. [PubMed: 21709130]
19. Fu M, et al. p300 and p300/cAMP-response element-binding protein-associated factor acetylate the androgen receptor at sites governing hormone-dependent transactivation. J. Biol. Chem. 2000; 275:20853–20860. [PubMed: 10779504]
20. Linja MJ, et al. Expression of androgen receptor coregulators in prostate cancer. Clin. Cancer Res. 2004; 10:1032–1040. [PubMed: 14871982]
21. Hawksworth D, et al. Overexpression of C-MYC oncogene in prostate cancer predicts biochemical recurrence. Prostate Cancer Prostatic Dis. 2010; 13:311–315. [PubMed: 20820186]
22. Ogiwara H, et al. Targeting p300 Addiction in CBP-Deficient Cancers Causes Synthetic Lethality by Apoptotic Cell Death due to Abrogation of MYC Expression. Cancer Discov. 2016; 6:430–445. [PubMed: 26603525]
23. Hnisz D, et al. Super-enhancers in the control of cell identity and disease. Cell. 2013; 155:934–947. [PubMed: 24119843]

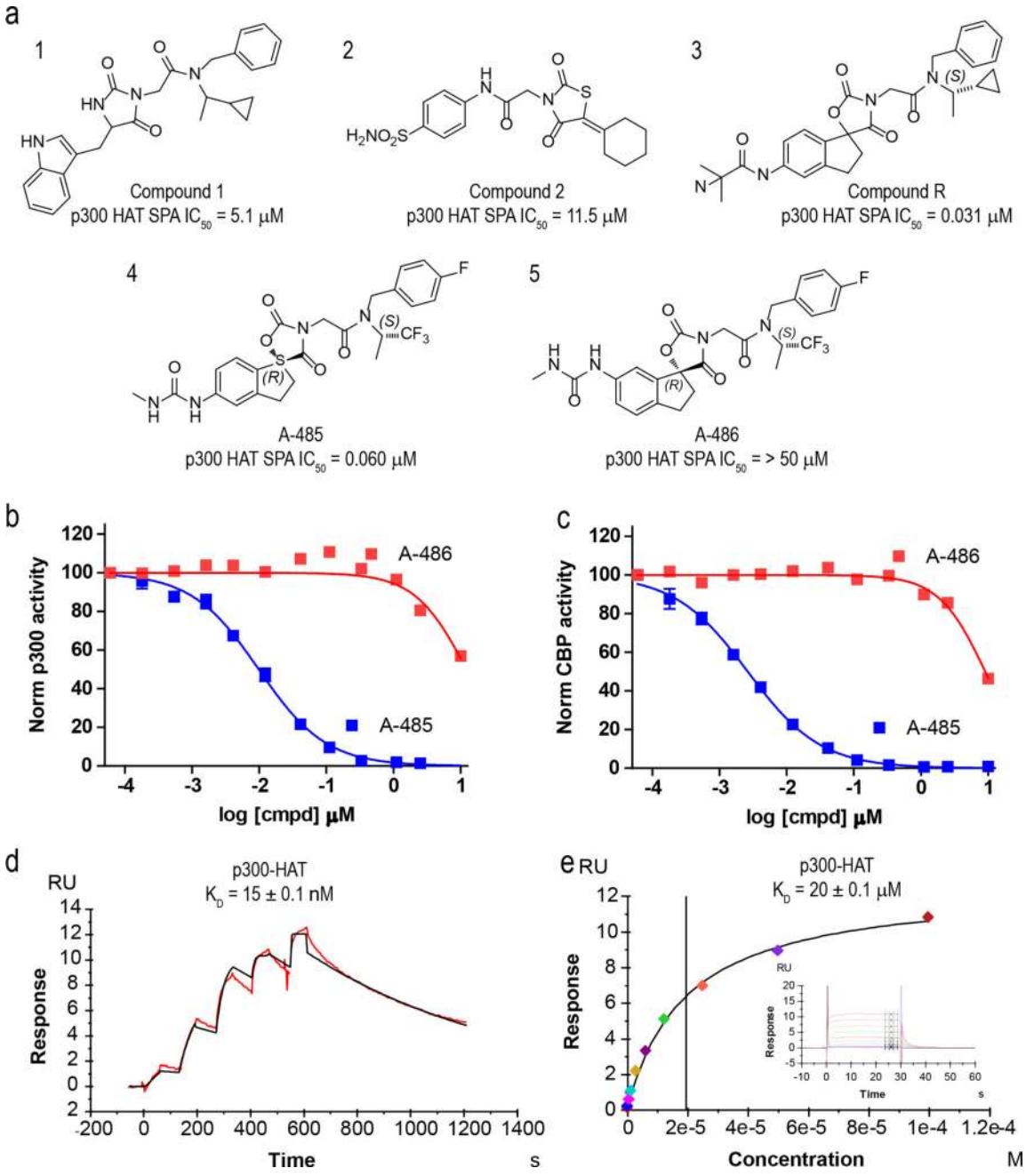

Figure 1. A-485 potently inhibits p300/CBP *in vitro*

(a) Chemical structures of screening hits (1,2), Compound R (3), A-485 (4) and the inactive control compound A-486 (5). (b,c) A-485 but not A-486 inhibits the acetyltransferase activities of p300-BHC (b) and CBP-BHC (c). The TR-FRET signal observed with DMSO control was normalized to 100. Error bars for A-485 represent the S.D. of 3 independent biological replicates; n=1 for A-486. (d,e) Representative p300 binding curves and fits of four independent biological replicates for p300-HAT binding in single-cycle mode with injection spikes removed (d) and steady-state evaluation for A-486 (e) via surface plasmon

resonance. The inset in (e) shows the corresponding binding curves from which the steady-state data was derived. Source data for (b-e) are provided.

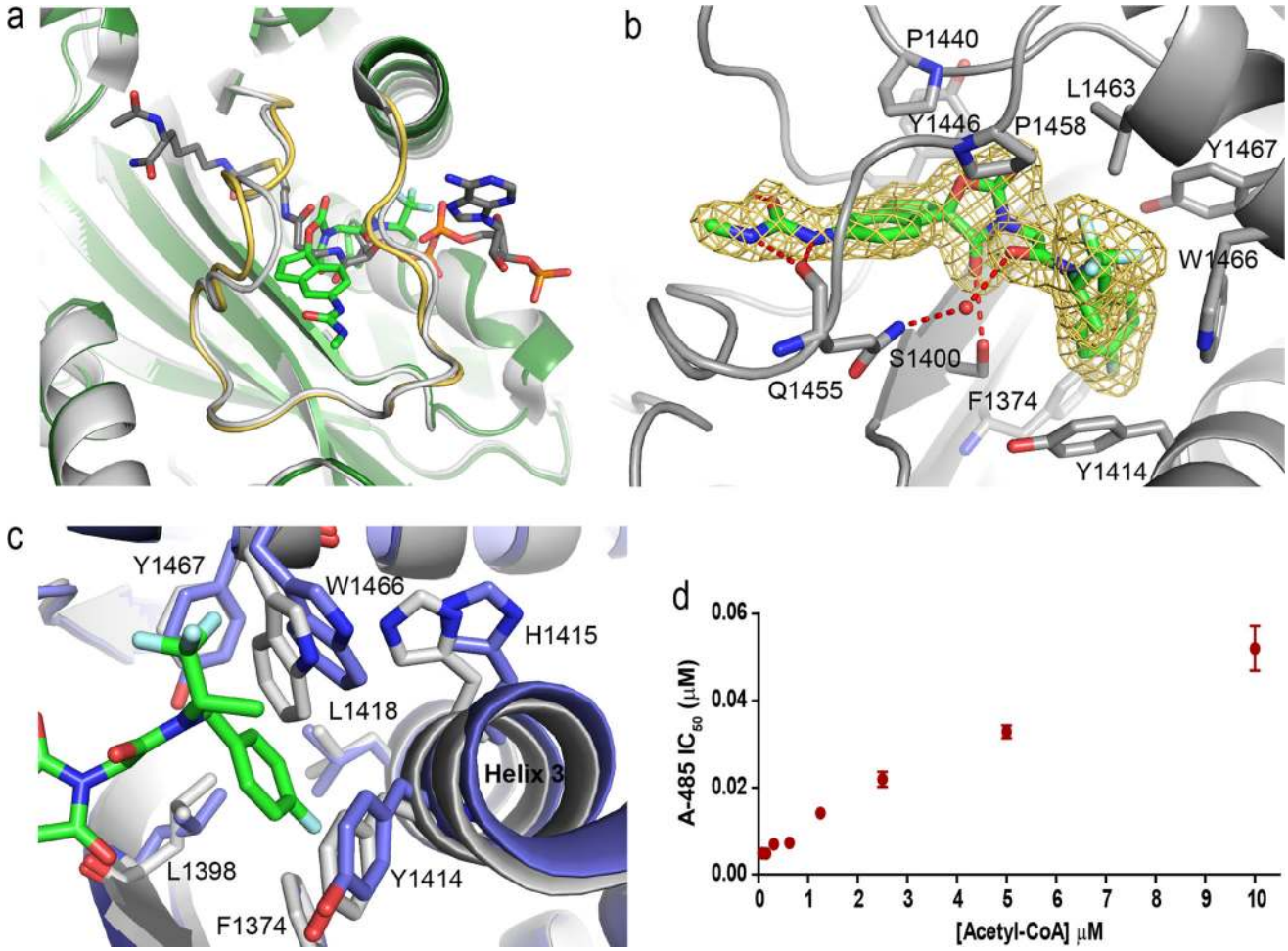

Figure 2. Crystal structure of A-485 bound to Δp300 HAT

(a) Superposition of the Δp300 HAT-A-485 complex (green) with the inactive Δp300 HAT Y1467F mutant complexed with the bi-substrate inhibitor Lys-CoA (PDB ID: 3BIY,gray). (b) Zoomed view of the A-485 binding site. Key interacting residues are shown with hydrogen bonds indicated by red dashes (some residues are omitted for viewing clarity). The 2Fo-Fc electron density map calculated at 1.95Å for A-485 is contoured at 1σ. (c) Comparison of the Δp300 HAT-A-485 complex (green) with the Acetyl-CoA bound structure (PDB ID: 4PZS) (gray) illustrates how a subtle shift in helix 3 accommodates the fluorophenyl ring in a hydrophobic pocket. (d) A-485 is a competitive acetyl-CoA-site p300 inhibitor. The IC_{50} for A-485 were calculated as per Fig. 1b. Error bars represent S.D. of 3 independent technical replicates (source data are provided).

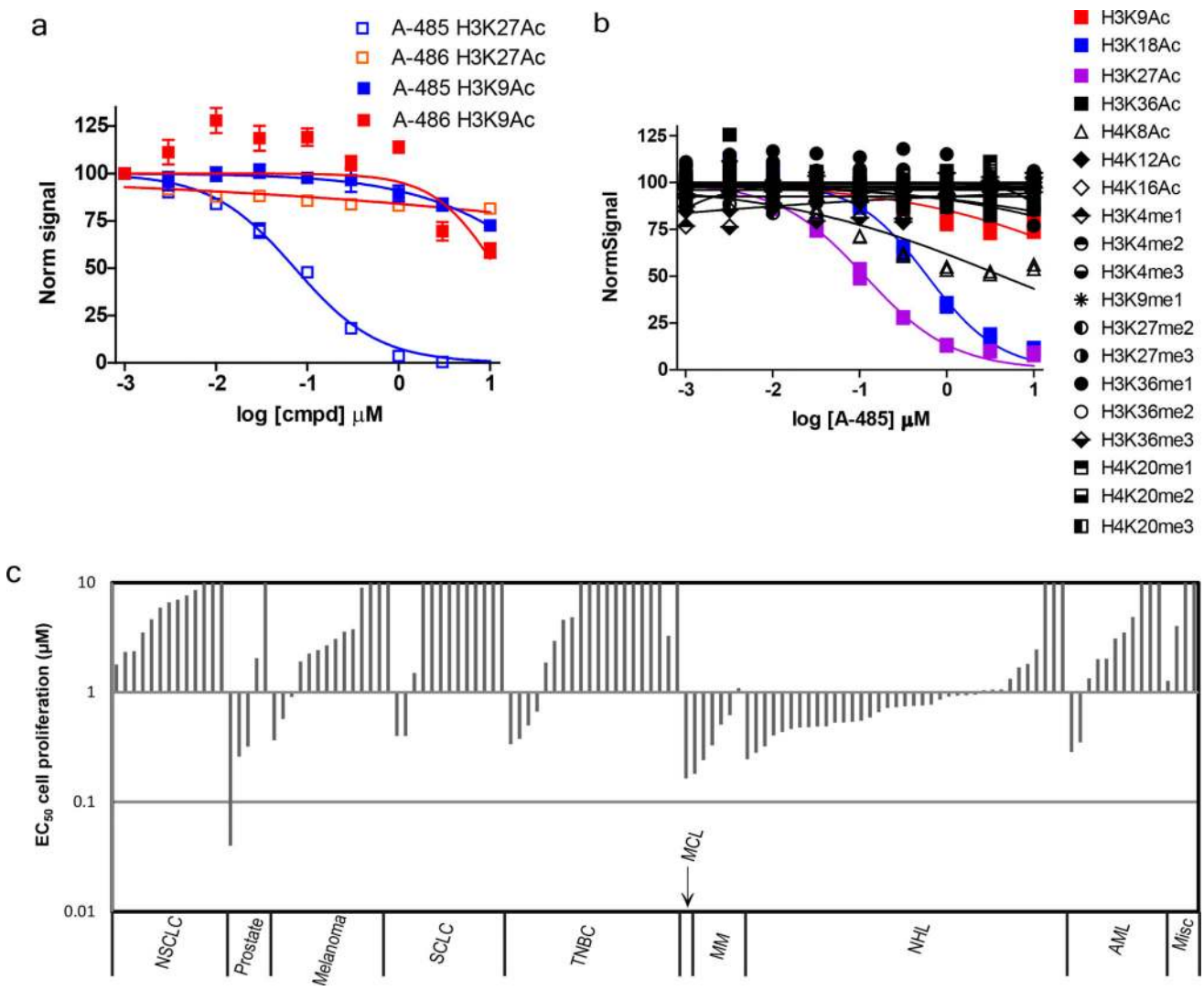

Figure 3. A-485 potently inhibits p300/CBP in cells

(a) Analysis of high content microscopy shows that A-485, but not the inactive control compound A-486 decreases H3K27Ac (open squares) but not H3K9Ac (closed squares) after 3 h treatment in PC-3 cells. Error bars represent the S.D. of 3 independent biological replicates. (b) A-485 is selective for the p300 substrates H3K27Ac and H3K18Ac over other epigenetic marks after 3 h treatment in PC-3 cells (n=2). The fluorescent intensity observed with DMSO control for the indicated histone epigenetic mark was normalized to 100 for (a,b). Source data for (a,b) are provided. (c) A-485 is selectively anti-proliferative in 10 different solid and hematological tumor types. Cell proliferation assays were performed as described in the online methods.

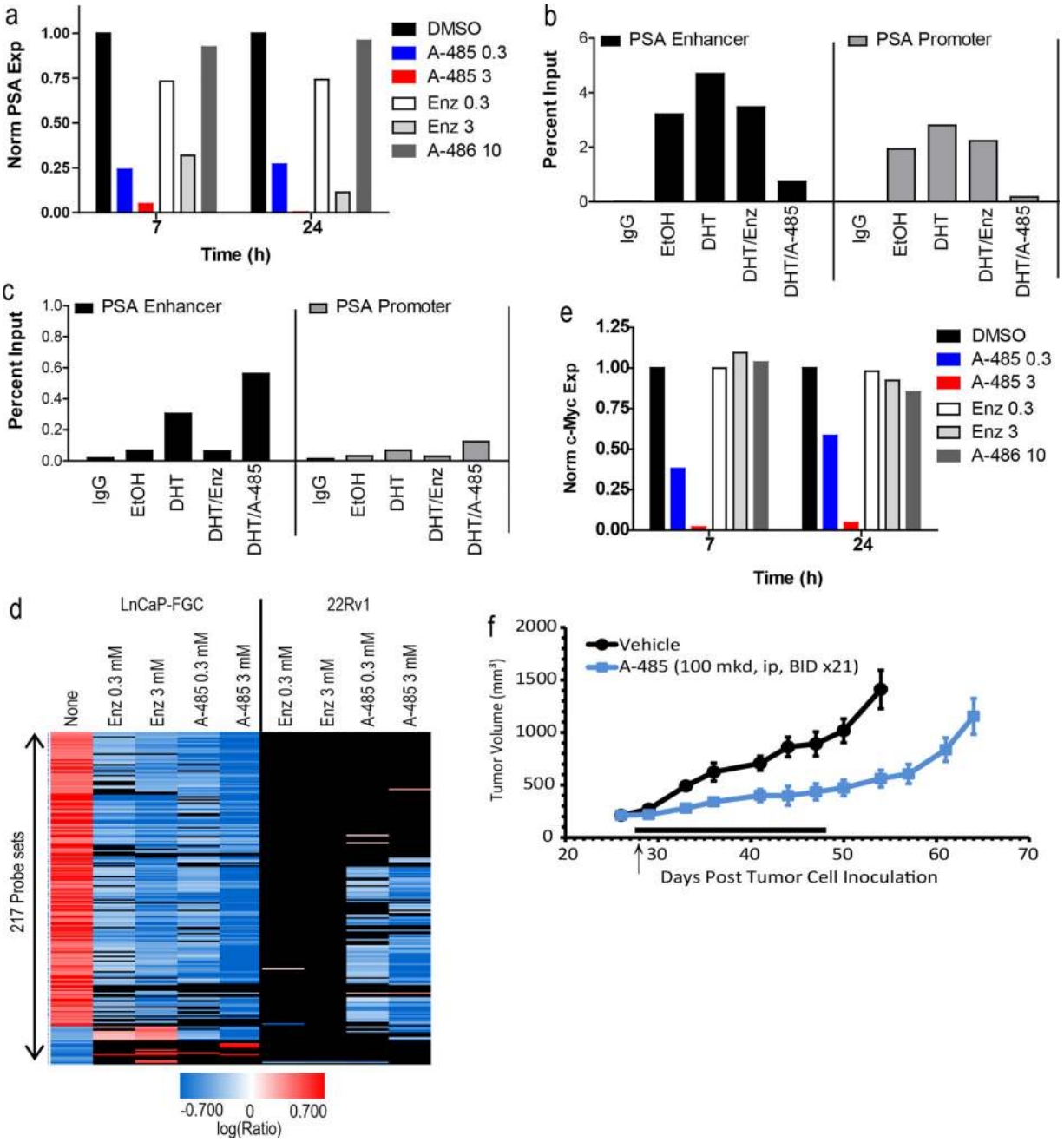

Figure 4. A-485 inhibits AR activity in prostate cancer

(a) qRT-PCR analysis shows that A-485 and enzalutamide (Enz) inhibit DHT-stimulated PSA mRNA expression in LnCaP-FGC cells (n=2 independent biological replicates; two technical replicates per experiment). The PSA expression (Exp) observed for the DMSO control was normalized to 1 using the Bio-Rad CFX 3.1 Manager software. (b,c) A-485 and Enz inhibit H3K27Ac occupancy at the PSA enhancer (b), but only Enz inhibits AR occupancy (c); n=2 independent biological replicates. (d) Comparison of A-485 and Enz on 217 genes modulated by DHT in the indicated cell line after 6 h treatment. (e) A-485 inhibits c-Myc expression in androgen depleted 22Rv1 cells (n=2 independent biological replicates).

c-Myc expression (Exp) in (e) was normalized as per (a). (f) A-485 is efficacious in the LuCaP-77 CR xenograft model. A-485 was dosed as indicated. Error bars represent the S.E.M. of n=8 animals per group. The black arrow denotes initiation of dosing and the black bar denotes the range of days animals were dosed. Source data for (a-c, e, f) are provided.